

Regulation of Persistent Activity by Background Inhibition in an *In Vitro* Model of a Cortical Microcircuit

Jean-Marc Fellous¹ and Terrence J. Sejnowski^{1,2}

¹Computational Neurobiology Laboratory, Howard Hughes Medical Institute, The Salk Institute for Biological Studies, La Jolla, CA 92037, USA and ²Department of Biology, University of California, San Diego, La Jolla, CA 92093, USA

We combined *in vitro* intracellular recording from prefrontal cortical neurons with simulated synaptic activity of a layer 5 prefrontal microcircuit using a dynamic clamp. During simulated *in vivo* background conditions, the cell responded to a brief depolarization with a sequence of spikes that outlasted the depolarization, mimicking the activity of a cell recorded during the delay period of a working memory task in the behaving monkey. The onset of sustained activity depended on the number of action potentials elicited by the cue-like depolarization. Too few spikes failed to provide enough NMDA drive to elicit sustained reverberations; too many spikes activated a slow intrinsic hyperpolarization current that prevented spiking; an intermediate number of spikes produced sustained activity. When high dopamine levels were simulated by depolarizing the cell and by increasing the amount of NMDA current, the cell exhibited spontaneous 'up-states' that terminated by the activation of a slow intrinsic hyperpolarizing current. The firing rate during the delay period could be effectively modulated by the standard deviation of the inhibitory background synaptic noise without significant changes in the background firing rate before cue onset. These results suggest that the balance between fast feedback inhibition and slower AMPA and NMDA feedback excitation is critical in initiating persistent activity and that the maintenance of persistent activity may be regulated by the amount of correlated background inhibition.

Introduction

Persistent neuronal activity drives many behaviors (Hebb, 1949). It is commonly found in many parts of the brain including different subfields of the hippocampus in rats (Wiebe *et al.*, 1997; Wiebe and Staubli, 2001) and monkeys (Colombo *et al.*, 1998), in the monkey ventral premotor area where cells continued to respond to the presence of an object, even when the light was turned off (Graziano *et al.*, 1997), in the brain stem during eye movements in monkeys (McFarland and Fuchs, 1992) and goldfish (Aksay *et al.*, 2001) and at several levels in the visual pathway and prefrontal cortices during working memory tasks in monkeys (Funahashi *et al.*, 1989; Fuster, 1990; Goldman-Rakic, 1995; Quintana and Fuster, 1999; Shadlen and Newsome, 2001; Casagrande *et al.*, 2002) and rats (Jung *et al.*, 1998; Pratt and Mizumori, 2001).

In the cortex, the dependence of individual action potentials on the activity of nearby neuron is unclear, but optical recordings from cat cortex *in vivo* (Tsodyks *et al.*, 1999) and calcium imaging from rat layer 5 neurons *in vitro* (Mao *et al.*, 2001) have demonstrated that the spontaneous and evoked activity in single cells can be strongly correlated with a spatial pattern of activity in a neighboring patch of cortex. This correlation results in part from the excitatory and inhibitory synaptic reverberations between groups of interconnected cells (Markram *et al.*, 1997; Melchitzky *et al.*, 1998; Gonzalez-Burgos *et al.*, 2000; Abeles and Gat, 2001) and together with the intrinsic properties in these

cells is thought to be the basis for persistent activity observed in the prefrontal cortex during working memory tasks (Durstewitz *et al.*, 2000; Wang, 2001). The exact nature of these reverberations, and their dependence on particular mixture of excitation and inhibition is uncertain. In particular, it is unknown how the level of persistent activity during the delay period can vary continuously in the same cell to code for a specific stimulus (Romo *et al.*, 1999; Aksay *et al.*, 2001).

The goal of this study is to recreate the *in vivo* conditions of an elementary prefrontal cortical microcircuit in an *in vitro* preparation by injecting simulated long-range synaptic background conductances and short-range excitatory and inhibitory feedback using the dynamic clamp technique. We study the conditions that lead to the onset of sustained reverberatory activity and determine some of the influences on the level of activity during the delay period.

Materials and Methods

In Vitro Experiments

Coronal slices of rat pre-limbic and infra-limbic areas of prefrontal cortex were obtained from 2 to 4 weeks old Sprague-Dawley rats. Rats were anesthetized with Isoflurane (Abbott Laboratories, IL) and decapitated. Their brain were removed and cut into 350 μm thick slices using standard techniques. Patch-clamp was performed under visual control at 30–32°C in a submerged chamber. In most experiments Lucifer Yellow (RBI, 0.4%) was added to the internal solution. In some experiments, synaptic transmission was blocked by D-2-amino-5-phosphonovaleric acid (D-APV; 50 μM), 6,7-dinitroquinoxaline-2,3, dione (DNQX; 10 μM), and bicuculline methiodide (bic; 20 μM). All drugs were obtained from RBI or Sigma, freshly prepared in ACSF and bath applied. Whole cell patch-clamp recordings were achieved using glass electrodes (4–10 M Ω) containing (mM): K₂SO₄, 140; HEPES, 10; NaCl, 4; EGTA, 0.1; Mg-ATP, 4; Mg-GTP, 0.3; phosphocreatine 14. Data were acquired in current clamp mode using an Axoclamp 2A amplifier (Axon Instruments, Foster City, CA). Extracellular stimulation (Fig. 1A,B) was conducted with a large tip (100 μm) bipolar electrode (FHC, Bowdoinham, ME) placed in layer 5, ~100 μm away from the cell's main axis. The electrode was attached to an analog stimulus isolation unit (Getting Instruments, Iowa City, IA) commanded by the data acquisition computer (see below). We used regularly spiking layer 5 pyramidal cells.

Data were acquired using two computers. One computer was used for standard data acquisition, current injection and extracellular stimulation. Programs were written using Labview 6.1 (National Instrument, Austin, TX), and data were acquired with a PCI16-E1 data acquisition board (National Instrument, Austin, TX). Data acquisition rate was either 10 or 20 kHz. The second computer was dedicated to real-time synaptic current injection (Fig. 1C). Programs were written using a Dapview (Microstar Laboratory, Bellevue, WA) front-end and a language C backend. A variant of the dynamic clamp (Sharp *et al.*, 1993; Hughes *et al.*, 1998; Jaeger and Bower, 1999) technique (see below) was implemented using a DAP-5216a board (Microstar Laboratory, Bellevue, WA) at a rate of 10 kHz connected to the Axoclamp 2A amplifier in current clamp mode.

All experiments were carried in accordance with animal protocols approved by the NIH.

A total of 35 pyramidal cells were used in this study. Data were analyzed offline using MATLAB (The Mathworks, Natick, MA). Results are given as mean \pm standard deviation.

Simulation of Synaptic Currents

To recreate *in vivo* conditions, simulated synaptic conductances were injected to the recorded cell. These conductances were divided into two groups:

The first group of conductances consisted in two Ornstein-Uhlenbeck processes mimicking the arrival of 16 563 glutamatergic and 3376 GABAergic synaptic inputs distributed on the dendritic tree of a recon-

structed multi-compartmental cortical cell, but measured at the soma (Destexhe *et al.*, 2001; Fellous *et al.*, 2003). Briefly,

$$I_{\text{background}}(t) = G_e(t)(V(t) - E_{\text{GLU}}) + G_i(t)(V(t) - E_{\text{GABA}})$$

where E_{GLU} and E_{GABA} are the reversal potentials for AMPA and GABA_A conductances (0 mV and -80 mV, respectively), and V is the instantaneous membrane voltage of the recorded pyramidal cell. The fluctuating conductances $G_e(t)$ and $G_i(t)$ are given by two Ornstein-Uhlenbeck processes (Uhlenbeck and Ornstein, 1930):

$$\frac{dG_e(t)}{dt} = -\frac{1}{\tau_e} [G_e(t) - G_{e0}] + \sqrt{D_e} \chi_1(t)$$

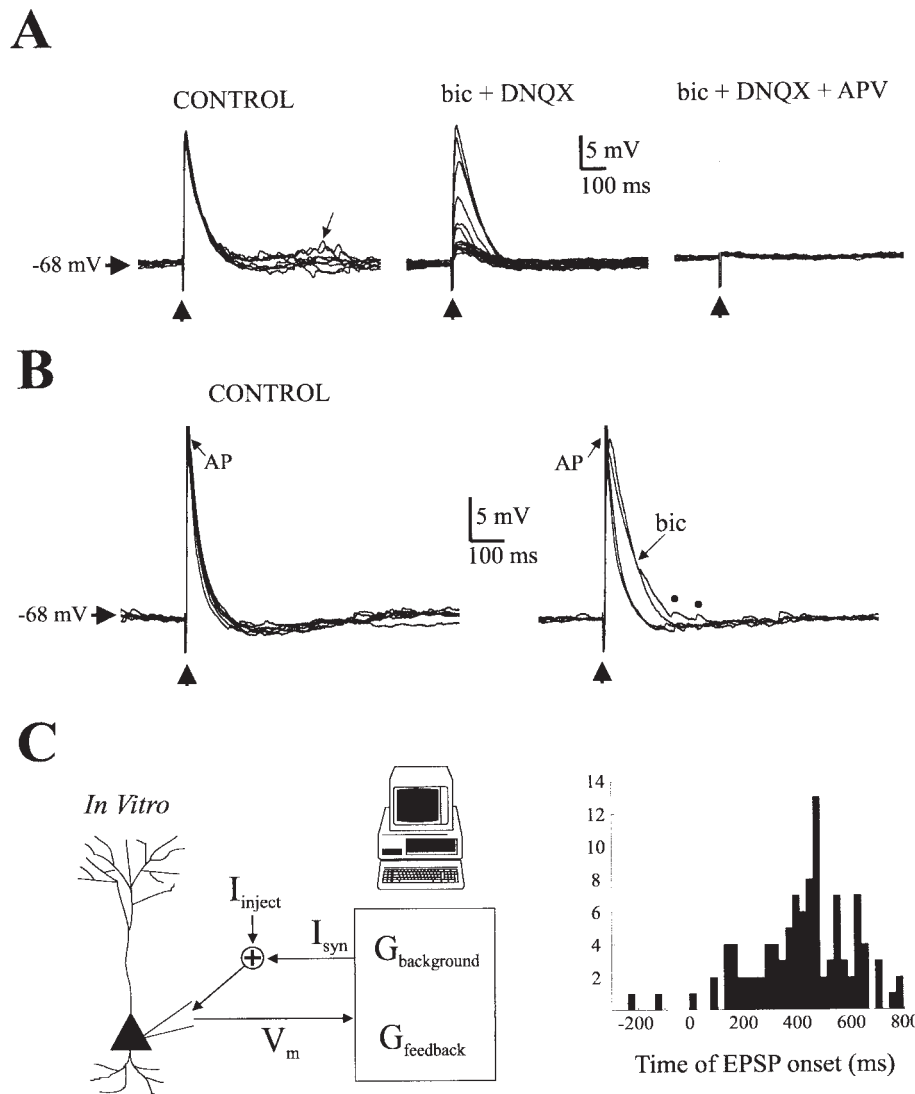


Figure 1. Evidence for reverberatory activity in the *in vitro* preparation. (A) Responses of a layer 5 pyramidal cell to a synaptic stimulation (up arrow) provided by an extracellular electrode placed $\sim 100 \mu\text{m}$ from the soma in layer 5. Left: control condition (eight superimposed traces). Note the presence of a trail of EPSPs following the monosynaptic response (arrow). Middle: The wash-in of bicuculline ($20 \mu\text{M}$) and DNQX ($10 \mu\text{M}$) reduced the amplitude of the monosynaptic response and suppressed the trail of EPSPs. Right: the remaining synaptic response was abolished by $50 \mu\text{M}$ APV indicating that it was mediated by NMDA receptor activation. (B) With sufficient stimulation, an action potential (AP) was evoked on top of the monosynaptic response. Left: In control conditions the width of the synaptic response was greatly reduced by the occurrence of the action potential (six superimposed traces). Right: bicuculline ($20 \mu\text{M}$) and DNQX ($5 \mu\text{M}$) was washed in, and DNQX was washout shortly after, while bicuculline remained in the bath alone. In this condition, for the same stimulation strength, the shape of the monosynaptic EPSP was similar to the shape of the EPSP in control condition when the cell was not spiking (A, left panel). Two traces in the control condition and two traces in the bicuculline conditions are plotted for comparison. These results indicate that the change in EPSP shape was due to a fast inhibitory component triggered by the cell's own spiking. Dots indicate spontaneous EPSPs riding on top of the monosynaptic response. (C) left: schematic illustration of our hybrid system. At each time step (0.1 ms), a dedicated computer computed the values of two synaptic conductances. The first $G_{\text{background}}$ mimicked the continuous background activity of distant cells; the second G_{feedback} was computed each time an action potential was emitted by the cell recorded *in vitro* (reactive clamp, see methods). Right: Histogram of the time of EPSP onsets from five cells placed in control conditions depicted in (A) left (103 onset times were recorded, mean 429 ms, ± 167 ms. Time 0 represents the stimulus onset). Panels (A) and (B) are from the same cell.

$$\frac{dGi(t)}{dt} = -\frac{1}{\tau_i}[Gi(t) - Gi_0] + \sqrt{D_i}\chi_2(t)$$

where Ge_0 and Gi_0 are average conductances, and τ_e and τ_i are time constants (2.7 ms and 10.7 ms, respectively, throughout this study), $\chi_1(t)$ and $\chi_2(t)$ are Gaussian white noise processes with unit standard deviation, D_e and D_i are the 'diffusion' coefficients. Ge and Gi are Gaussian variables with standard deviations $\sigma_e = \sqrt{(D_e\tau_e)/2}$ and $\sigma_i = \sqrt{(D_i\tau_i)/2}$, respectively. The procedure used for numerical integration of these stochastic equations is detailed elsewhere (Destexhe *et al.*, 2001). Because of the slow dynamics of NMDA channels, and the large number of glutamatergic synapses taken into consideration, their contribution was approximated by a change in the mean level of inputs (Ge_0 and Gi_0).

These conductances were injected using the dynamic clamp technique continuously through out the duration of the recordings (typically 30–180 min long).

The second group of conductances was injected using dynamic clamp in a reactive mode in response to each action potential generated by the cell currently being recorded ('reactive clamp').

$$I_{\text{feedback}}^{(t)} = G_{\text{AMPA}}^{(t)}(V(t) - E_{\text{GLU}}) + G_{\text{NMDA}}^{(t)}(V(t) - E_{\text{GLU}}) + G_{\text{GABA}}^{(t)}(V(t) - E_{\text{GABA}})$$

such that if $V(t) > 0$ (an action potential occurred) two Poisson sequences of synaptic release times were generated for glutamatergic and GABAergic synapses, respectively. Each sequence was computed such that

$$\forall n \in [1 \dots N], t_n = t_{n-1} - a \ln(1 - r)$$

with $t_0 = d$.

N , a and d are the number of synapses simulated, the mean inter-spike interval (ISI) and the deadtime, respectively. The variable r is a random number uniformly distributed between 0 and 1. The feedback excitatory postsynaptic potentials (EPSPs) were modeled as the response of a single cell representative of a population. Because each action potential of the recorded cell represented the synchronous firing of a small population of cells, it was assumed that the resulting postsynaptic effects were reliable rather than probabilistic. Excitatory AMPA and NMDA components were generated by a population of 40 reliable synapses together constituting a Poisson train of EPSPs with mean interval of 15 ms and a deadtime of 100 ms. Because the average synaptic interval of 15 ms (66 Hz) corresponds to the discharge of 40 cells, each of these feedback cells is assumed to fire only once during $15 \times 40 = 600$ ms immediately following a single spike by the real cell. For each spike of the real cell, one and only one feedback EPSP/spike from each of the 40 cells is generated, so that in principle the firing rate of each of the simulated microcircuit feedback cells is always kept identical to the firing rate of the real cell (no matter what this firing rate is). The synapses did not include short-term depression or facilitation. The conductance ratio of AMPA/NMDA excitatory synapses was 2–5 (McAllister and Stevens, 2000; Watt *et al.*, 2000) so that AMPA and NMDA EPSPs had typical amplitudes of 1.5 and 0.5 mV, respectively. Feedback IPSPs were generated by a population of five reliable GABAergic synapses with a mean interval of 10 ms and a deadtime of 15 ms. In 6/21 exploratory experiments these values were set empirically so that excitatory mean intervals and deadtimes ranged from 12 to 18 ms and 90 to 150 ms, respectively, and inhibitory mean intervals and deadtimes ranged from 8 to 12 ms and 10 to 20 ms, respectively. The results obtained under these conditions were qualitatively similar to those obtained with the chosen standard intervals and deadtimes mentioned above.

When an action potential was detected, the conductance for each receptor type was modified in order to account for the new synaptic releases such that

$$G(t) = G_{\text{new}}(t) = G_{\text{old}}(t) + G_{\text{max}} \sum_{n=1}^N g(t - t_n)$$

where $g(t)$ was an alpha function of time constant 2.7 ms for AMPA synapses, 70 ms for NMDA synapses and 10 ms for GABA_A synapses. Both

AMPA and NMDA conductances shared the same t series (co-activation of NMDA and AMPA receptors). G_{max} was the maximal conductance for each respective receptor type and could be adjusted by the experimenter. In the text, this quantity was referred to as G_{AMPA} , G_{GABA} and G_{NMDA} . In the case of NMDA channels, however, G_{max} was voltage dependent (Jahr and Stevens, 1990) and was expressed as

$$G_{\text{max}} = \frac{G_{\text{NMDA}}}{1 + \frac{\text{Mg}}{3.57} e^{-0.062V}}$$

with Mg expressed in mM (here Mg = 2).

Results

Reverberatory activity in prefrontal cortex was elicited by stimulating the afferents to a neuron recorded intracellularly *in vitro*. The extracellular stimulating electrode was placed in layer 5, ~100 μm from the cell body of the recorded neuron. In the control medium, the stimulation elicited a monosynaptic compound EPSP of ~15 mV amplitude followed by a trail of multisynaptic EPSPs. These EPSPs were not affected by bath application of bicuculline (20 μM , not shown) but were greatly reduced by the application of DNQX (10 μM) that left only a monosynaptic NMDA component (Fig. 1A middle panel). The application of APV (50 μM) abolished the response entirely (Fig. 1A right panel). These results were qualitatively reproduced in 5/7 cells and indicated that afferent stimulations were followed by long latencies excitatory inputs from neighboring pyramidal cells. These EPSPs could occur early and overlap with the repolarizing phase of the compound EPSP (see for example dots in Fig. 1B right panel), or could occur as late as 700 ms after stimulus onset, well after the compound EPSPs terminated. Figure 1C (right panel) shows the distribution of the onset times of the EPSP barrage measured in five cells [mean 429 ms \pm 167 ms ($n = 103$)] by fitting an alpha function to the feedforward compound EPSP, subtracting it from each trace, and measuring peak voltages of individual feedback EPSPs. Part of these EPSPs may be directly related to the cell's own spiking, but it is likely that most are due to multi-synaptic reverberations from other cells that have been simultaneously activated by the extracellular electrode. Because onset times during monosynaptic EPSPs (Fig. 1B right, dots) could not be measured, Figure 1C underestimates the amount of feedback EPSPs occurring in the first 200 ms after stimulus delivery. Because the voltage dependence of the NMDA channel conductance (*in vitro* the cell had a resting membrane potential typically at -70 mV), and due to the relatively small size of NMDA EPSCs, the feedback NMDA components were not observed.

For a sufficiently strong stimulating current, the monosynaptic EPSP elicited an action potential (Fig. 1B). This changed the shape of the EPSP and its width was reduced by ~50%. Synaptic blockers were applied to assess whether this change in shape was due to intrinsic currents such as I_{AHP} or to a synaptic currents. DNQX (10 μM) and APV (50 μM) had no effect on the shape of the response when rescaled to match its amplitude in control conditions (3/3 cell tested, not shown). However, bath application of bicuculline (20 μM) increased the width of the response by ~50% in 4/4 cells (Fig. 1B right, to avoid epileptic-like discharges, bicuculline was first applied with DNQX 5 μM , and DNQX was washed out), and the shape of the compound EPSP was no different than in control conditions when the cell was not producing an action potential (Fig. 1A, left). This suggests that the action potential triggered a fast feedback inhib-

itory response that changed the shape of the compound EPSP. Because the onset times of the feedback IPSCs could not be directly measured, due to the monosynaptic response, we estimated their distribution (mean $40 \text{ ms} \pm 20 \text{ ms}$).

We used a dynamical clamp technique (Sharp *et al.*, 1993) to explore the influence of presynaptic feedback on cortical neurons. A neuron was recorded using the patch recording technique in current clamp mode. A dedicated computer was programmed to detect the occurrence of an action potential (voltage crossing 0 mV) and to dynamically react to each action potential by generating a train of mixed IPSCs and EPSCs that was injected in the neuron. The time distribution of the simulated excitatory synaptic events was assumed to be Poisson with a mean and dead time matching the experimental data in Figure 1C (right).

Figure 2A left shows the feedback response to an action potential elicited by a square pulse of current (I_{inject}). The middle trace shows the sum of the injected pulse and the volley of EPSCs (AMPA only) resulting from the simulated feedback. The top trace shows the resulting membrane voltage (compare with Fig. 1A, left; the action potentials have been truncated). Note the presence of some spontaneous (real) EPSPs on some of the trials (arrows). The real and simulated EPSPs were qualitatively indistinguishable.

The GABA_A inhibitory feedback synaptic currents were distributed in time according to our experimental estimates (Fig. 1B). These IPSCs were generated by a population of five interneurons simulating the activity of Calbindin D-28k (CB) immunoreactive inhibitory cells that have local dendritic arbors and are believed to provide specific inhibition to the cortical module to which they belong (Conde *et al.*, 1994; Gabbott and

Bacon, 1996a,b; Gabbott *et al.*, 1997; Krimer and Goldman-Rakic, 2001). The conductance of these synapses was adjusted to mimic the experimental observations (Fig. 1B), and to provide fast and reliable feedback inhibition after each action potential (Krimer and Goldman-Rakic, 2001). Their mean discharge ISI was set to 10 ms with a deadtime of 15 ms. Figure 2 (right) shows the compound feedback injected by the reactive clamp in response to one elicited spike. A fast initial GABA component is followed by a slow NMDA mediated component topped by AMPA EPSPs. Note that this curve is somewhat different from the data shown in Figure 1 (Control). The trail of EPSPs in Figure 1 is lower in amplitude and the NMDA depolarization is smaller. The difference is due to the fact that the reactive clamp models the *in vivo* situation where all the cells of the microcircuits are healthy and where all synaptic connections are functional. This is unlikely to be true *in vitro*. The fast GABA inhibition visible after the spike (Fig. 2) is more pronounced than in Figure 1, because the experimental data includes a powerful feedforward compound EPSP that partially masks inhibition.

Cells *in vivo* have large subthreshold membrane fluctuations (standard deviation of $\sim 4 \text{ mV}$), a mean potential typically around -60 mV , spontaneous and irregular firing ($0.3\text{--}2 \text{ Hz}$ in prefrontal cortex with a coefficient of variation approaching 1.0), and a low input resistance ($\sim 40 \text{ M}\Omega$) (Paré *et al.*, 1998; Destexhe and Paré, 1999; Fellous *et al.*, 2003). These properties arise from the background synaptic inputs coming from other cells in the circuit. These aspects of *in vivo* activity can be effectively recreated in the *in vitro* preparation (Destexhe *et al.*, 2001) by injecting the excitatory and inhibitory background synaptic activity as random conductance processes (see Methods) into a neuron using a dynamical clamp. The mean and standard devi-

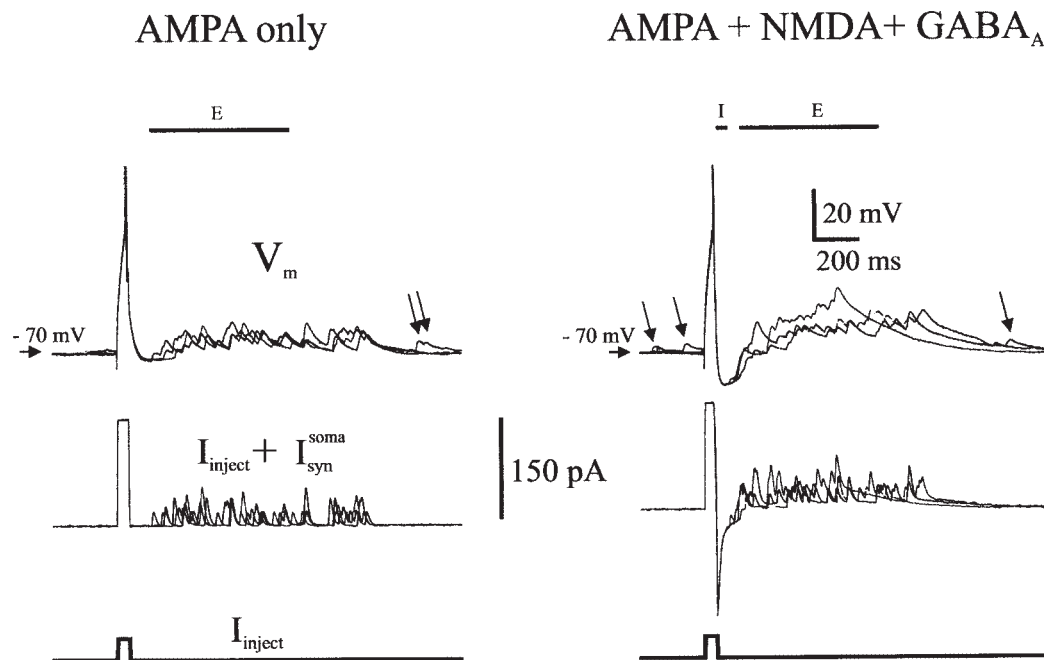


Figure 2. Examples of reactive clamp response to one action potential. Left: Responses to AMPA conductances only (three superimposed traces); right: Responses to mixed AMPA, NMDA and GABA_A conductances (four superimposed traces). Values for synaptic conductances were $G_{\text{AMPA}} = 2.1 \text{ nS}$ (left and right panels), $G_{\text{NMDA}} = 0.4 \text{ nS}$, $G_{\text{GABA}} = 7.1 \text{ nS}$ (right panel only). Lower traces represent the current pulse injected to the cell to initiate a single action potential. The middle trace represents the sum of the current pulse, and the current computed and injected by the reactive clamp. The upper trace shows the membrane potential of the cell. Note the presence of spontaneous EPSPs (arrows). The horizontal bars labeled I and E indicate the average time course of the inhibitory and excitatory feedback inputs, respectively.

ation of these conductances were adjusted to yield *in vivo* like activity.

Figure 3A shows an example of a cell recorded *in vitro*, to which synaptic background activity was added ($G_{e_0} = 10$ nS, $G_{i_0} = 21$ nS, $\sigma_e = 3$ nS, $\sigma_i = 7.5$ nS). The cell fired at 0.4 Hz (0.46 ± 0.1 , $n = 19$) with a CV of 0.71 (0.72 ± 0.1 , $n = 16$), its membrane potential was depolarized to -66 mV (-64.3 ± 1.53 , $n = 19$) the membrane showed large fluctuations of 4.1 mV standard deviation (4.3 ± 0.8 , $n = 19$) and its input resistance was 42 M Ω (37.9 ± 6.4 , $n = 19$), without the noise the resting membrane potential was -71 mV (-69.8 ± 3.1 , $n = 19$) and its input resistance was 184 M Ω (157 ± 32 , $n = 19$). The lower trace shows the

background synaptic current computed by the dynamic clamp. Note the presence of action potentials in the injected current trace, a hallmark of the dynamical clamp technique. The synaptic background noise represented the aggregate activity of a large population of pyramidal cells and interneurons located outside the cortical module where the cell was located. Unlike the feedback activity presented in Figure 2, this activity was assumed to not depend on the specific firing pattern of the cell recorded, and its parameters (mean and standard deviation of excitatory and inhibitory processes) were typically kept constant.

When the model of the cortical feedback was added along with synaptic background activity, the cell exhibited short and fast sequences of action potentials riding on a small NMDA-mediated feedback depolarization ($G_{AMPA} = 1.5$ nS, $G_{NMDA} = 0.5$ nS, $G_{GABA} = 6.0$ nS). These sequences lasted typically less than 2 s (1.3 s \pm 0.5 s, $n = 47$, four cells, Fig. 3B lower trace, arrow) and the firing rate increased to *in vivo* like values (1.2 Hz \pm 0.64, $n = 19$). Because of the introduction of short ISIs, the CV increased to values typically observed *in vivo* (0.92 ± 0.2 , $n = 16$) (Softky and Koch, 1993; Holt *et al.*, 1996; Shadlen and Newsome, 1998). Since the model of the synaptic background activity was derived from *in vivo* intracellular data in the anesthetized animal, the cells modeled here reflect baseline levels of dopamine (Paré *et al.*, 1998; Fellous *et al.*, 2003). Recent *in vitro* studies demonstrated that high level of dopamine increased the excitability of PFC cells (Yang and Seamans, 1996; Shi *et al.*, 1997; Henze *et al.*, 2000), and increased the amount of NMDA current (Cepeda *et al.*, 1993; Zheng *et al.*, 1999; Seamans *et al.*, 2001b) received through extracellular stimulation. An increase in the average membrane potential (+5 mV) and an increase in the feedback NMDA current (+30%) mimicking the effect of higher dopamine levels, yielded an increase in the occurrence and duration of the fast sequences (Fig. 3B). Typically, these sequences resembled spontaneous dopamine-dependent ‘up-states’ observed *in vivo* in prefrontal cortex (Lewis and O’Donnell, 2000) (see also Seamans *et al.*, 2003) and lasted substantially longer (3.2 s \pm 0.9, $n = 61$, five cells) than in baseline conditions and the CV increased slightly (1.1 ± 0.1 , $n = 9$). In our preparation they were initiated by a fast sequence of action potentials that recruited a large excitatory feedback. They were terminated by the activation of a slow hyperpolarizing intrinsic current (Fig. 3B right, open arrow). This current was not pharmacologically characterized in this study; however, because it is primarily activated after a large amount of spiking (see also Fig. 5), it is likely to include a calcium-activated potassium current. Note the typical occurrence of large inhibitory events resulting from the random synchrony between feedback inhibition and background synaptic inhibition (Fig. 3B, closed arrows in the voltage and low-pass filtered synaptic current trace). In the remainder of this study, cells were placed in a regime of baseline dopamine levels, analogous to Figure 3B, left.

In a typical working memory task, these cells are transiently activated by the presentation of a cue, and continue to fire for several seconds after the cue has been removed, until the behavioral response is initiated. In order to assess the ability of a PFC cortical module to sustain activity, we simulated the cue and behavioral response phases of a working memory task by positive and negative current injection, respectively. In Figure 4A, a PFC cell placed in realistic *in vivo* conditions fired in a sustained manner, long after the cue stimulus was turned off, until the simulated response was triggered ($G_{e_0} = 12$ nS, $G_{i_0} = 20$ nS, $\sigma_e =$

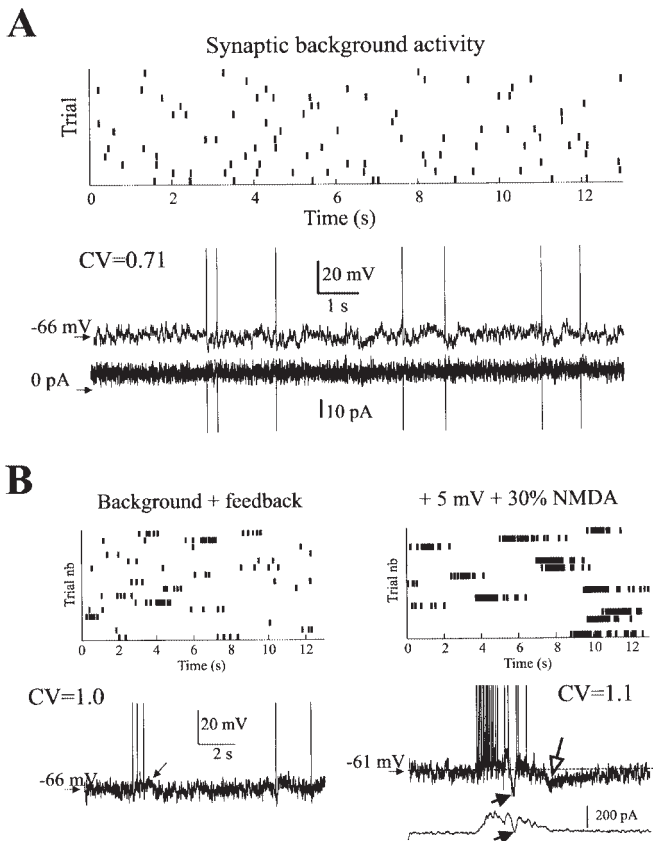


Figure 3. Spontaneous spiking of a layer 5 pyramidal cell undergoing background and feedback synaptic noise. (A) Example of a cell undergoing synaptic background noise only ($G_{e_0} = 10$ nS, $G_{i_0} = 21$ nS, $\sigma_e = 3$ nS, $\sigma_i = 7.5$ nS). The rastergram shows the spiking activity of this cell during 182 s (represented as 14 trials of 13 s each). An example of the membrane voltage is shown below. The current computed by the dynamic clamp is shown below the voltage trace. In this condition, the CV of this cell was 0.71. (B) Left. The synaptic feedback component of the reactive clamp was added to the condition of panel (A) ($G_{AMPA} = 1.5$ nS, $G_{NMDA} = 0.5$ nS, $G_{GABA} = 6.0$ nS). Note the presence of fast sequences of action potentials in the rastergram. The lower trace shows a voltage trace with one of these fast sequences. Note that the sequence terminates while the cell was still in a depolarized state. Right: The cell was depolarized by 5 mV, and the conductance of the feedback NMDA current was increased by 30%, simulating the effects of high doses of bath applied dopamine. The cell now shows ‘up-states’ consisting in the spontaneous occurrence of sustained activity lasting typically longer than a second (see rastergram). A sample voltage trace is shown below the rastergram, together with the low-pass filtered (50 Hz cut off) synaptic current computed by the reactive clamp. Note the occurrence of large hyperpolarizing events in the voltage and current traces (filled arrows), and the presence of a slow intrinsic (not found in the synaptic current trace) hyperpolarizing current that terminates the up-state (open arrow). In this condition the CV was 1.1 due to the introduction of very fast ISIs. All panels are from the same cell.

2.8 nS, $\sigma_i = 7.1$ nS, $G_{\text{AMPA}} = 1.6$ nS, $G_{\text{NMDA}} = 0.5$ nS, $G_{\text{GABA}} = 6.8$ nS). This behavior was elicited in 21 of the 32 cells tested. Note the presence of random occurrence of large inhibition when synaptic background and feedback components were synchronous (Fig. 4A arrow). In these cells, the firing rate during the delay period was typically lower than during the presentation of the cue. Two of the 32 cells tested were strongly adapting and could not be stimulated to produce sustained activity while in a regime of spontaneous background similar to the ones observed *in vivo*. In nine cells the short cue-depolarization failed to promote sustained spiking, and instead activated the slow hyperpolarization previously noted (Fig. 4B). In those cells, the firing rate during the delay period was decreased.

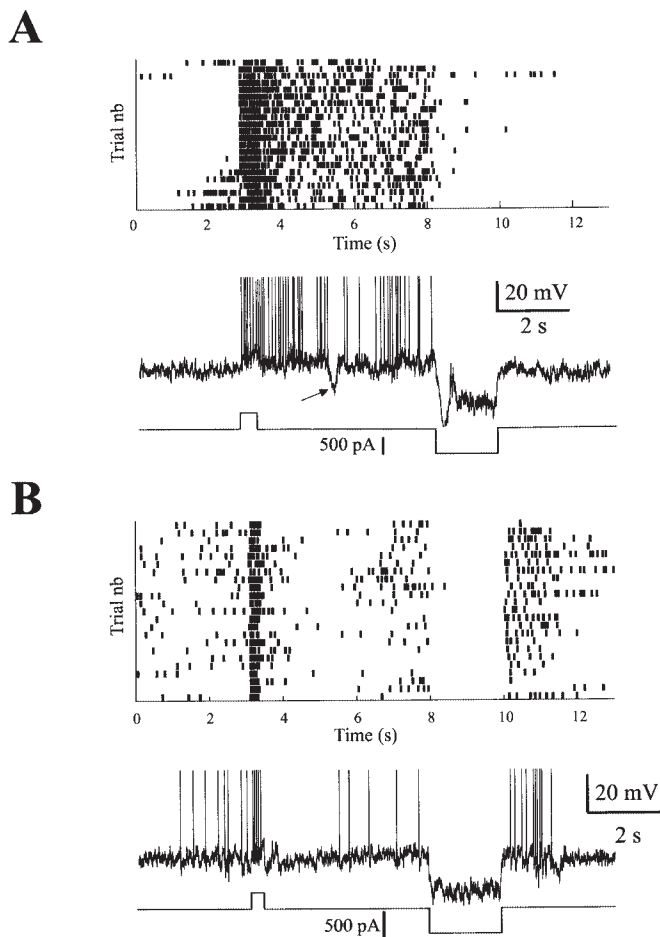


Figure 4. Simulated delayed match-to-sample task in layer 5 pyramidal cells. (A) A pyramidal cell was placed in *in vivo* like conditions by injecting background synaptic inputs ($G_{e_0} = 12$ nS, $G_{i_0} = 20$ nS, $\sigma_e = 2.8$ nS, $\sigma_i = 7.1$ nS, $51 \text{ M}\Omega$ input resistance) and reactive feedback ($G_{\text{AMPA}} = 1.6$ nS, $G_{\text{NMDA}} = 0.5$ nS, $G_{\text{GABA}} = 6.8$ nS). The cell was then injected with a current pulse lasting 400 ms simulating the 'cue' and a hyperpolarizing current pulse lasting 1.8 s simulating the response. The cell showed sustained firing for the duration of the delay period (4.5 s). Note the occurrence of large inhibitory events (arrow) resulting from the random synchronization between background and feedback inhibition. The background firing rate of the cell was 1.1 Hz, its firing rate during the delay period was 6.2 Hz, the rastergram shows 18 of 44 trials. (B) A different pyramidal cell placed in *in vivo* like conditions ($G_{e_0} = 13$ nS, $G_{i_0} = 22$ nS, $\sigma_e = 3.1$ nS, $\sigma_i = 7$ nS, $G_{\text{AMPA}} = 1.5$ nS, $G_{\text{NMDA}} = 0.4$ nS, $G_{\text{GABA}} = 7.0$ nS, $43 \text{ M}\Omega$ input resistance) showed a decrease in firing in response to the cue (cue lasted 300 ms, response lasted 2 s). The background firing rate of this cell was 1.3 Hz, the firing during the delay period was 0.7 Hz. The rastergram shows 23 trials.

A detailed analysis of the trials during which sustained activity was not achieved revealed that sustained activity depended strongly on the number of action potentials generated during the cue period (Fig. 5). For a low number of action potentials (1–4 in Fig. 5A), or for action potentials sequences of large ISIs, the reverberatory activity was not sufficient to trigger additional spikes, as occurs during spontaneous activity (Fig. 3B left). A large number of action potentials (7–8 in Fig. 5B) activated an intrinsic slow hyperpolarizing current that kept the cells below threshold, despite a large amount of synaptic feedback. For intermediate amount of spiking (5–6 in Fig. 5B), the activity of the cell could be sustained for several seconds. Group data on five cells matched for their input resistance ($40 \text{ M}\Omega \pm 6$ when undergoing synaptic background) and background firing rate ($0.7 \text{ Hz} \pm 0.4 \text{ Hz}$) revealed that persistent activity optimally

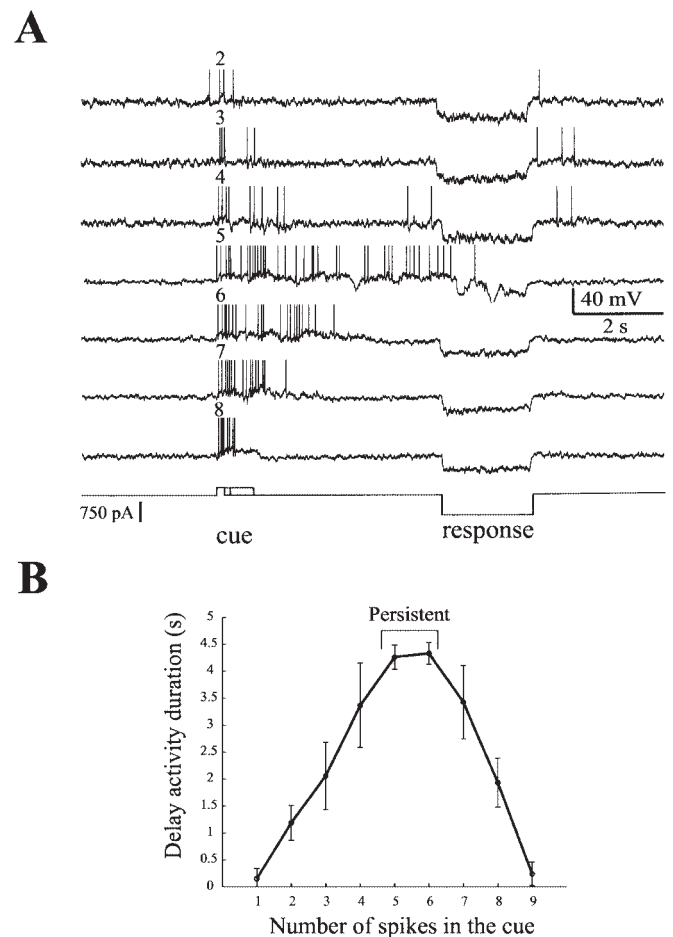


Figure 5. The maintenance of sustained activity during the delay period depended on the number of action potentials emitted during the cue. (A) A pyramidal cell was injected with cues of varying duration (200, 300 or 800 ms) in order to elicit a variable number of action potentials (1–9). Seven representative traces are shown, illustrating the spiking activity during the delay period when 2 (top) to 8 (bottom) actions potentials were elicited during the cue. Note that this cell showed sustained firing only if ~5 spikes were elicited during the cue ($G_{e_0} = 14$ nS, $G_{i_0} = 25$ nS, $\sigma_e = 3.0$ nS, $\sigma_i = 7.9$ nS, $G_{\text{AMPA}} = 1.5$ nS, $G_{\text{NMDA}} = 0.5$ nS, $G_{\text{GABA}} = 8.0$ nS, $41 \text{ M}\Omega$ input resistance). (B) Group data for five cells matched for their input resistance ($40 \text{ M}\Omega \pm 6$) and background firing rate ($0.7 \text{ Hz} \pm 0.4$). The curve shows the average duration of the spiking activity after the cue offset, as a function of the number of action potentials generated during the cue. Persistent activity was most reliably achieved for five and six actions potentials.

occurred when 5 or 6 action potentials were generated during the cue period (Fig. 5B).

Prefrontal cortical pyramidal cells recorded *in vivo* during working memory tasks show a wide range of firing rates during the delay period. In the same cell, firing rates might vary from baseline levels for non-preferred stimuli, to firing rates 10 times larger than control for preferred stimuli (Goldman-Rakic, 1995). Others modulate their firing rate in relation to the luminance of distracting stimuli (Constantinidis *et al.*, 2001). The gain of pyramidal cells depends on the standard deviation of the excitatory and inhibitory synaptic background noise that they receive (Chance *et al.*, 2002; Fellous *et al.*, 2003). In prefrontal cortical cells, an increase in the standard deviation of the background inhibitory inputs (σ_i) mimicking an increase in inhibitory correlation was particularly effective in modifying the shape of the input/output curve of pyramidal cells recorded *in vitro* under *in vivo* like conditions (Fellous *et al.*, 2003). Figure 6A shows an example of the influence of σ_i on the response of a cell that was placed in the nominal conditions of our experiments (Fig. 3B left, $G_{e0} = 23$ nS, $G_{i0} = 31$ nS, $\sigma_e = 2.5$ nS, $\sigma_i = 6.5$ nS, $G_{AMPA} = 1.2$ nS, $G_{NMDA} = 0.6$ nS, $G_{GABA} = 6.0$ nS, the standard deviation of the membrane potential was 3.1 mV). As σ_i increased, the maximal value of the firing rate increased, and the slope of the frequency/current curve increased so that for low input current the firing remained relatively unchanged, and for higher current intensity the firing rate in the two conditions became significantly different going from 20 Hz to ~40 Hz (the standard deviation of the membrane potential was increased to 5.3 mV, primarily in the hyperpolarizing direction). Firing rates were computed from 3 s long current injections (excluding the first 500 ms). For low σ_i value (6.5 nS) the cell exhibited a background firing rate of 0.5 Hz, and a delay firing rate of ~8 Hz. When σ_i was increased to 25 nS, the background firing rate did not change significantly (0.9 Hz) while the firing rate during the delayed period increased to 31 Hz (Fig. 6B). The signal-to-noise ratio in this cell could therefore be tuned and was increased in this experiment by ~110% by increasing σ_i . Similar results were obtained for three other pyramidal cells with increases in signal-to-noise ratios of 20%, 32% and 59%. These results suggest that the amount of correlation in the background inhibitory inputs might be key to determining the firing rate of the cell during the delay period.

Discussion

Based on experimental observation of cortical reverberation, we simulated the synaptic feedback activity of a prefrontal microcircuit of pyramidal cells and interneurons and injected the compound synaptic conductance into a neuron recorded *in vitro* using the dynamic clamp technique. In addition, we injected simulated background synaptic inputs so that cells had an input resistance, membrane fluctuations, firing rate and firing variability comparable to those found *in vivo*. In simulated baseline conditions, the cell responded to a brief depolarization with an increase in firing rate that outlasted the depolarization, mimicking the activity of a cell responding to its preferred stimulus during the delay period of a working memory task in the behaving monkey. Some cells showed 'off' responses and their firing rate decreased during the delay period due to the activation of a slow intrinsic hyperpolarizing current.

In the rat prefrontal cortex *in vivo*, 'up states' are synaptically driven events that depend on putative cortico-cortical NMDA

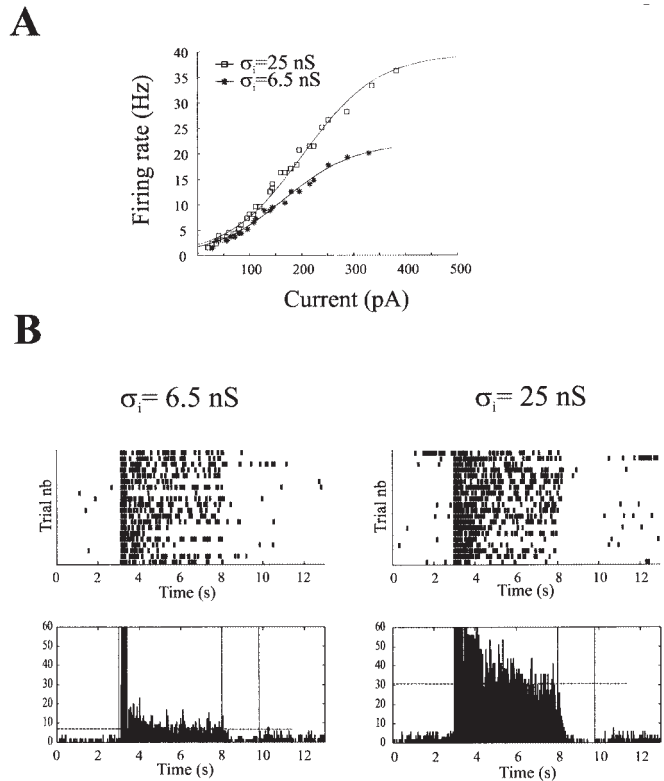


Figure 6. The firing rate during the delay period activity can be modulated by the correlation of the background inhibitory synaptic noise. (A) Average firing rate of a pyramidal cell in response to 3 s long current pulses of varying amplitude for low ($\sigma_i = 6.5$ nS, stars) and high ($\sigma_i = 25$ nS, open squares) standard deviation of the background synaptic noise ($G_{e0} = 23$ nS, $G_{i0} = 31$ nS, $\sigma_e = 2.5$ nS, $G_{AMPA} = 1.2$ nS, $G_{NMDA} = 0.6$ nS, $G_{GABA} = 6.0$ nS, 37 M Ω input resistance). This standard deviation corresponds to the amount of correlation in the background synaptic inputs (Fellous *et al.*, 2003). (B) The same cell was injected with cue and response pulses to simulate its activity during a DMS task. When σ_i was low, the cell sustained activity at 8 Hz during the delay period, and its background firing rate before the cue was 0.5 Hz. When σ_i was high, the cell sustained activity at 31 Hz and its background activity before the cue was 0.9 Hz.

and AMPA receptor activation. Their length is increased by VTA induced dopamine release (Lewis and O'Donnell, 2000) (see also Seamans *et al.*, 2003). Our results explain this finding by suggesting that up-states rely on prompt NMDA-dependent excitatory feedback within a small population of interconnected neurons (Fig. 3B left). Modulation by dopamine depolarizes the cells, increases NMDA currents and results in a lengthening of the 'up' states (Fig. 3B right). The properties of up/down states observed differ in some respects from those observed *in vivo*. First, pyramidal cells in our preparation increase their firing rates in the 'up' states after simulated DA modulation, while the firing rate decreases *in vivo* (Lewis and O'Donnell, 2000). This may have occurred because we did not model the complex influence of DA on interneurons (Seamans *et al.*, 2001a) or on somato-dendritic integration (Yang and Seamans, 1996); Second, our down states are more depolarized, show larger membrane potential fluctuations and occasional spiking, unlike in the anesthetized animal *in vivo* where the membrane is strongly hyperpolarized with little fluctuations and no spiking (Lewis and O'Donnell, 2000). However, we attempted to model the conditions in alert animals, where synaptic activity is more intense than in the anesthetized preparation. Furthermore, recent work on an *in vitro* model of up and down state has

shown that in down states some neurons exhibited spontaneous spiking rates as high as 6 Hz (Shu *et al.*, 2003). In this study, excitatory and inhibitory conductances were in precise balance during the up state which is compatible with our qualitative observations that too little or too much inhibitory feedback (or too much or too little excitatory feedback) would result in epileptic-like discharges or the cessation of sustained activity, respectively (not shown).

These results suggest mechanisms underlying each phase of a working memory task. Persistent activity was initiated by fast AMPA depolarization, maintained by slow NMDA-mediated depolarization, and limited by feedback GABA inputs. The initiation relied on the presence of a fast sequence of spikes that generated enough feedback NMDA current to promote sustained spiking. Too few spikes failed to elicit sustained reverberations, and too many spikes activated a slow hyperpolarization current that prevented further spiking. In our preparation, the optimal number of spikes was between 5 and 6. However, the number of spikes *in vivo* during a cue period preceding sustained activity may be higher. The reason for the difference may be that cells *in vivo* are in a non-zero neuromodulatory state (acetylcholine and dopamine, at least). One of the general effects of these substances is to increase the excitability of the cells, and decrease their AHP currents. Such neuromodulation would not change the basic inverted U shape of the curve (which is due on the left to not enough excitatory drive, and on the right to the activation of a AHP current), but is likely to shift it to the right (and probably widen it as well). This could explain why in the behaving animal the optimal number of spike during the cue could be significantly higher than in our preparation. The pharmacological introduction of dopamine into the preparation could be used to explore these issues but was not within the scope of this study.

In the optimal regime, the cue-like depolarization resulted in an immediate, strong feedback inhibition, followed and counterbalanced by a feedback NMDA current that repolarized the cell and made it spike again. During the period of sustained activity the cell received a balanced mixture of excitatory and inhibitory currents. Because the inhibition was desynchronized during this period (owing to the variability of the cell spiking), it did not terminate the cell's activity, but simply limited its firing rate. The cell responded to the cue by transiently elevating its firing rate, and responded during the delay period by maintaining a firing rate higher than before the cue as seen in the alert behaving monkey *in vivo* (Goldman-Rakic, 1995). Note that not all the cells that are part of the feedback microcircuit need to receive the initial cue input. Such cells (modeled here only by their feedback EPSPs) would be entrained by those that receive the cue information but would only fire during the delay period, as seen *in vivo* (Goldman-Rakic, 1995). The firing rate during the delay period could be effectively modulated by changing the amplitude of the fluctuations in the inhibitory background conductance noise without significantly changing the background firing rate before cue onset. This change in the makeup of the background noise has been shown to modify the gain of the input/output curve (Chance *et al.*, 2002; Fellous *et al.*, 2003) and to make the cell more sensitive to transient inputs as short as 30 ms long (Fellous *et al.*, 2003). In contrast to an injection of a prolonged pulse-like depolarization into a PFC cell, which elicits repetitive spiking that will decrease and eventually stop after a few (>10) seconds, the injection of a fluctuating current of the same mean amplitude will elicit spiking for as long as the

stimulus lasts. A spike-triggered average analysis of those discharges show that the 'preferred' pre-spike stimulus is a hyperpolarization followed shortly by a depolarization (Mainen and Sejnowski, 1995). When an inhibitory fluctuation creates a hyperpolarization (de-inactivating Na currents), less depolarization is needed to elicit a spike (Fellous *et al.*, 2003).

A prolonged hyperpolarizing pulse [simulating a inhibitory barrage of synaptic inputs to the microcircuit following the response phase in a working memory task (Constantinidis *et al.*, 2002)] terminated activity by bringing the excitatory feedback synaptic input below a critical level (as in the left part of the inverted U-shaped curve in Fig. 5B).

These results are contingent on several assumptions made by the model including the exact number of reverberatory synapses used, and their dynamics. Light microscopy anatomical studies of the rat medial prefrontal cortex indicated that there were ~80 pyramidal cells and ~16 interneurons in a prefrontal cortical module (50 × 50 μm) (Gabbott and Bacon, 1996a,b; Gabbott *et al.*, 1997). Since ~40 of these 80 pyramidal cells are in layer 5/6, and since most layer 5/6 cells are connected to other layer 5/6 cells, our population of synapses modeled the excitatory feedback within a single cortical module (Melchitzky *et al.*, 1998). Further work is needed to study the behavior of the model under different quantitative assumptions that might differentiate the prefrontal cortex with other cortical or subcortical areas that also exhibit persistent activity. We also assumed that synapses were reliable and did not include short-term plasticity. Recent work has shown, however, that these dynamics may be of functional relevance in removing or restoring temporal correlations within spike trains (Goldman *et al.*, 2002) and further work is required to assess their impact on the neural basis of persistent activity.

Although this study focused on the sustained activity in the prefrontal cortex during a working memory task, it may apply to other systems and behaviors and can shed light on the functional nature of local microcircuits in other parts of the cortex. A cortical cell receives at least two functionally distinct kinds of inhibition: the first is provided in a feedforward manner by the background synaptic noise generated by distant microcircuits. This input varies slowly and its standard deviation (amount of correlation) modulates the gain the postsynaptic cell. The second kind of inhibition is local to the microcircuit and its role is to control the amount of reverberation within the microcircuit by feedback. Recent experimental evidence supports the presence of feedforward and feedback inhibition during working memory tasks (Constantinidis *et al.*, 2002), and further experimental and theoretical studies are required to test this hypothesis.

Notes

Patricia Goldman-Rakic was a wonderful colleague whose discoveries and stimulating conversations motivated our research. We dedicate this paper to her memory.

Address correspondence to Jean-Marc Fellous· Computational Neurobiology Laboratory, Howard Hughes Medical Institute, The Salk Institute for Biological Studies, La Jolla, CA 92037, USA. Email: fellous@salk.edu.

References

- Abeles M, Gat I (2001) Detecting precise firing sequences in experimental data. *J Neurosci Methods* 107:141–154.
- Aksay E, Gamkrelidze G, Seung HS, Baker R, Tank DW (2001) In vivo intracellular recording and perturbation of persistent activity in a neural integrator. *Nat Neurosci* 4:184–193.

- Casagrande VA, Xu X, Sary G (2002) Static and dynamic views of visual cortical organization. *Prog Brain Res* 136:389–408.
- Cepeda C, Buchwald NA, Levine MS (1993) Neuromodulatory actions of dopamine in the neostriatum are dependent upon the excitatory amino acid receptor subtypes activated. *Proc Natl Acad Sci USA* 90:9576–9580.
- Chance FS, Abbott LF, Reyes AD (2002) Gain modulation from background synaptic input. *Neuron* 35:773–782.
- Colombo M, Fernandez T, Nakamura K, Gross CG (1998) Functional differentiation along the anterior–posterior axis of the hippocampus in monkeys. *J Neurophysiol* 80:1002–1005.
- Conde F, Lund JS, Jacobowitz DM, Baimbridge KG, Lewis DA (1994) Local circuit neurons immunoreactive for calretinin, calbindin D-28k or parvalbumin in monkey prefrontal cortex: distribution and morphology. *J Comp Neurol* 341:95–116.
- Constantinidis C, Franowicz MN, Goldman-Rakic PS (2001) The sensory nature of mnemonic representation in the primate prefrontal cortex. *Nat Neurosci* 4:311–316.
- Constantinidis C, Williams GV, Goldman-Rakic PS (2002) A role for inhibition in shaping the temporal flow of information in prefrontal cortex. *Nat Neurosci* 5:175–180.
- Destexhe A, Paré D (1999) Impact of network activity on the integrative properties of neocortical pyramidal neurons in vivo. *J Neurophysiol* 81:1531–1547.
- Destexhe A, Rudolph M, Fellous JM, Sejnowski TJ (2001) Fluctuating synaptic conductances recreate in vivo-like activity in neocortical neurons. *Neuroscience* 107:13–24.
- Durstewitz D, Seamans JK, Sejnowski TJ (2000) Neurocomputational models of working memory. *Nat Neurosci* 3(Suppl):1184–1191.
- Fellous J-M, Rudolph M, Destexhe A, Sejnowski TJ (2003) Variance detection and gain modulation in an in-vitro model of in-vivo activity. *Neuroscience* (in press).
- Funahashi S, Bruce CJ, Goldman-Rakic PS (1989) Mnemonic coding of visual space in the monkey's dorsolateral prefrontal cortex. *J Neurophysiol* 61:331–349.
- Fuster JM (1990) Behavioral Electrophysiology of the prefrontal cortex of the primate. In: *The prefrontal cortex: its structure, function and pathology* (Uylings HBM, Van Eden CG, De Bruin JPC, Corner MA, Feenstra MGP, eds), pp. 313–324. Amsterdam: Elsevier.
- Gabbott PL, Bacon SJ (1996a) Local circuit neurons in the medial prefrontal cortex (areas 24a,b,c, 25 and 32) in the monkey. I. Cell morphology and morphometrics. *J Comp Neurol* 364:567–608.
- Gabbott PL, Bacon SJ (1996b) Local circuit neurons in the medial prefrontal cortex (areas 24a,b,c, 25 and 32) in the monkey. II. Quantitative areal and laminar distributions. *J Comp Neurol* 364:609–636.
- Gabbott PL, Dickie BG, Vaid RR, Headlam AJ, Bacon SJ (1997) Local-circuit neurones in the medial prefrontal cortex (areas 25, 32 and 24b) in the rat: morphology and quantitative distribution. *J Comp Neurol* 377:465–499.
- Goldman MS, Maldonado P, Abbott LF (2002) Redundancy reduction and sustained firing with stochastic depressing synapses. *J Neurosci* 22:584–591.
- Goldman-Rakic PS (1995) Cellular basis of working memory. *Neuron* 14:477–485.
- Gonzalez-Burgos G, Barrionuevo G, Lewis DA (2000) Horizontal synaptic connections in monkey prefrontal cortex: an in vitro electrophysiological study. *Cereb Cortex* 10:82–92.
- Graziano MS, Hu XT, Gross CG (1997) Coding the locations of objects in the dark. *Science* 277:239–241.
- Hebb DO (1949) *The organization of behavior*. New York: Wiley.
- Henze DA, Gonzalez-Burgos GR, Urban NN, Lewis DA, Barrionuevo G (2000) Dopamine increases excitability of pyramidal neurons in primate prefrontal cortex. *J Neurophysiol* 84:2799–2809.
- Holt GR, Softky WR, Koch C, Douglas RJ (1996) Comparison of discharge variability in vitro and in vivo in cat visual cortex neurons. *J Neurophysiol* 75:1806–1814.
- Hughes SW, Cope DW, Crunelli V (1998) Dynamic clamp study of Ih modulation of burst firing and delta oscillations in thalamocortical neurons in vitro. *Neuroscience* 87:541–550.
- Jaeger D, Bower JM (1999) Synaptic control of spiking in cerebellar Purkinje cells: dynamic current clamp based on model conductances. *J Neurosci* 19:6090–6101.
- Jahr CE, Stevens CF (1990) A quantitative description of NMDA receptor-channel kinetic behavior. *J Neurosci* 10:1830–1837.
- Jung MW, Qin Y, McNaughton BL, Barnes CA (1998) Firing characteristics of deep layer neurons in prefrontal cortex in rats performing spatial working memory tasks. *Cereb Cortex* 8:437–450.
- Krimer LS, Goldman-Rakic PS (2001) Prefrontal microcircuits: membrane properties and excitatory input of local, medium, and wide arbor interneurons. *J Neurosci* 21:3788–3796.
- Lewis BL, O'Donnell P (2000) Ventral tegmental area afferents to the prefrontal cortex maintain membrane potential 'up' states in pyramidal neurons via D(1) dopamine receptors. *Cereb Cortex* 10:1168–1175.
- Mainen ZF, Sejnowski TJ (1995) Reliability of spike timing in neocortical neurons. *Science* 268:1503–1506.
- Mao BQ, Hamzei-Sichani F, Aronov D, Froemke RC, Yuste R (2001) Dynamics of spontaneous activity in neocortical slices. *Neuron* 32:883–898.
- Markram H, Lubke J, Frotscher M, Roth A, Sakmann B (1997) Physiology and anatomy of synaptic connections between thick tufted pyramidal neurones in the developing rat neocortex. *J Physiol* 500:409–440.
- McAllister AK, Stevens CF (2000) Nonsaturation of AMPA and NMDA receptors at hippocampal synapses. *Proc Natl Acad Sci USA* 97:6173–6178.
- McFarland JL, Fuchs AF (1992) Discharge patterns in nucleus prepositus hypoglossi and adjacent medial vestibular nucleus during horizontal eye movement in behaving macaques. *J Neurophysiol* 68:319–332.
- Melchitzky DS, Sesack SR, Pucak ML, Lewis DA (1998) Synaptic targets of pyramidal neurons providing intrinsic horizontal connections in monkey prefrontal cortex. *J Comp Neurol* 390:211–224.
- Paré D, Shink E, Gaudreau H, Destexhe A, Lang EJ (1998) Impact of spontaneous synaptic activity on the resting properties of cat neocortical pyramidal neurons in vivo. *J Neurophysiol* 79:1450–1460.
- Pratt WE, Mizumori SJ (2001) Neurons in rat medial prefrontal cortex show anticipatory rate changes to predictable differential rewards in a spatial memory task. *Behav Brain Res* 123:165–183.
- Quintana J, Fuster JM (1999) From perception to action: temporal integrative functions of prefrontal and parietal neurons. *Cereb Cortex* 9:213–221.
- Romo R, Brody CD, Hernandez A, Lemus L (1999) Neuronal correlates of parametric working memory in the prefrontal cortex. *Nature* 399:470–473.
- Seamans JK, Gorelova N, Durstewitz D, Yang CR (2001a) Bidirectional dopamine modulation of GABAergic inhibition in prefrontal cortical pyramidal neurons. *J Neurosci* 21:3628–3638.
- Seamans JK, Durstewitz D, Christie BR, Stevens CF, Sejnowski TJ (2001b) Dopamine D1/D5 receptor modulation of excitatory synaptic inputs to layer V prefrontal cortex neurons. *Proc Natl Acad Sci USA* 98:301–306.
- Seamans JK, Nogueira L, Lavin A (2003) Synaptic basis of persistent activity in prefrontal cortex in vivo and in organotypic cultures. *Cereb Cortex* 13:1242–1250.
- Shadlen MN, Newsome WT (1998) The variable discharge of cortical neurons: implications for connectivity, computation, and information coding. *J Neurosci* 18:3870–3896.
- Shadlen MN, Newsome WT (2001) Neural basis of a perceptual decision in the parietal cortex (area LIP) of the rhesus monkey. *J Neurophysiol* 86:1916–1936.
- Sharp AA, O'Neil MB, Abbott LF, Marder E (1993) Dynamic clamp: computer-generated conductances in real neurons. *J Neurophysiol* 69:992–995.
- Shi WX, Zheng P, Liang XF, Bunney BS (1997) Characterization of dopamine-induced depolarization of prefrontal cortical neurons. *Synapse* 26:415–422.
- Shu Y, Hasenstaub A, McCormick DA (2003) Turning on and off recurrent balanced cortical activity. *Nature* 423:288–293.
- Softky WR, Koch C (1993) The highly irregular firing of cortical cells is inconsistent with temporal integration of random EPSPs. *J Neurosci* 13:334–350.

- Tsodyks M, Kenet T, Grinvald A, Arieli A (1999) Linking spontaneous activity of single cortical neurons and the underlying functional architecture. *Science* 286:1943-1946.
- Uhlenbeck GE, Ornstein LS (1930) On the theory of Brownian motion. *Phys Rev* 36:823-841.
- Wang XJ (2001) Synaptic reverberation underlying mnemonic persistent activity. *Trends Neurosci* 24:455-463.
- Watt AJ, van Rossum MC, MacLeod KM, Nelson SB, Turrigiano GG (2000) Activity coregulates quantal AMPA and NMDA currents at neocortical synapses. *Neuron* 26:659-670.
- Wiebe SP and Staubli UV (2001) Recognition memory correlates of hippocampal theta cells. *J Neurosci* 21:3955-3967.
- Wiebe SP, Staubli UV, Ambros-Ingerson J (1997) Short-term reverberant memory model of hippocampal field CA3. *Hippocampus* 7:656-665.
- Yang CR, Seamans JK (1996) Dopamine D1 receptor actions in layers V-VI rat prefrontal cortex neurons in vitro: modulation of dendritic-somatic signal integration. *J Neurosci* 16:1922-1935.
- Zheng P, Zhang XX, Bunney BS, Shi WX (1999) Opposite modulation of cortical N-methyl-D-aspartate receptor-mediated responses by low and high concentrations of dopamine. *Neuroscience* 91:527-535.